IEEE Photonics Journal
An IEEE Photonics Society Publication

Open Access

Polymer on Quartz Waveguide Sensing Platform for Enhanced Evanescent Fluorescence Spectroscopy

Volume 10, Number 6, December 2018

Jalal Abdul-Hadi
Marc A. Gauthier
Muthukumaran Packirisamy

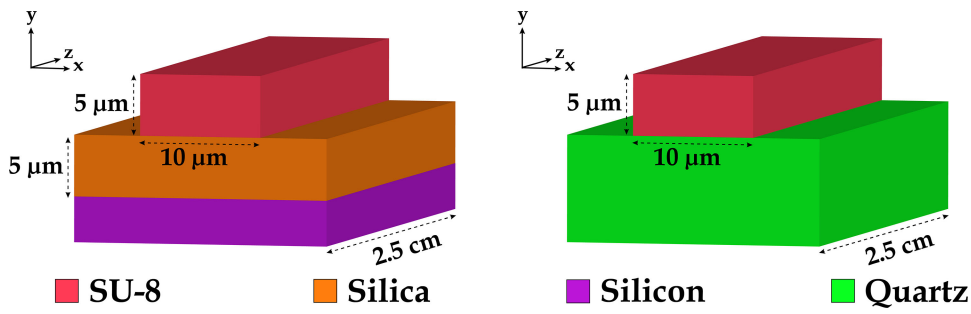

DOI: 10.1109/JPHOT.2018.2876380
1943-0655

Polymer on Quartz Waveguide Sensing Platform for Enhanced Evanescent Fluorescence Spectroscopy

Jalal Abdul-Hadi,[1,2] Marc A. Gauthier [1], and Muthukumaran Packirisamy [2]

[1]Institut National de la Recherche Scientifique (INRS), EMT Research Center, Varennes QC J3X 1S2, Canada
[2]Optical Bio-Microsystems Laboratory, Department of Mechanical and Industrial Engineering, Concordia University, Montreal QC H3G 1M8, Canada

DOI:10.1109/JPHOT.2018.2876380

Manuscript received August 16, 2018; accepted October 7, 2018. Date of publication October 17, 2018; date of current version November 20, 2018. This work was supported by NSERC-RGPIN-2015-04254 and NSERC Discovery and Concordia Research Chair. Corresponding author: Muthukumaran Packirisamy (e-mail: pmuthu@alcor.concordia.ca).

Abstract: This paper presents the study of the performance of a novel SU-8 waveguide on a quartz substrate for evanescent fluorescence spectroscopy. The sensitivity of the sensing platform (SU-8/quartz) was compared to an SU-8 waveguide on silica fabricated with the standard protocol. The physical properties of the SU-8/quartz waveguide resulting from a novel fabrication process allowed for a higher fluorescence coupling and lower optical losses than the SU-8/silica waveguide. The impact of the different indices of refraction of both waveguides on the fluorescence collection efficiency was calculated with three-dimensional finite-difference time-domain simulations by simulating randomly oriented and phased dimensionless current dipoles in the vicinity of their sensing layers. An evanescent fluorescence spectroscopy experiment was performed with different concentrations of Alexa-647 labeled-BSA proteins immobilized on the two polymer waveguides to compare the sensitivity of both sensing platforms. The SU-8/quartz waveguide revealed to have a higher calculated fluorescence collection efficiency and also a greater measured fluorescence light output compared to the SU-8/silica waveguide.

Index Terms: Biotechnology, microfabrication, optical device fabrication, soft lithography, spectroscopy, fluorescence, optical sensors, biophotonics, optical polymers, finite difference methods, biosensors, optical waveguides, propagation losses

1. Introduction

Optical sensing by means of fluorescence labeling is widely used to determine the concentration of analytes with different platforms and techniques [1], [2]. Although sensing using evanescent waves is also used for absorbance measurements, a higher sensitivity and specificity could be achieved by combining the technique with fluorescent labeling. Indeed, fluorescence evanescent wave spectroscopy exploits the evanescent wave of the guided light to excite fluorophore-labeled analytes in close proximity to the waveguide surface. Optical fibers are popular platforms to be used for fluorescence evanescent wave spectroscopy for remote or on-site sensing [3], [4]. However to use optical fibers for evanescent wave sensing has some drawbacks. The cladding of the fiber has

to be etched to expose the core of the fiber to the sample so that the evanescent wave can reach the labeled analyte. This renders the fiber structurally fragile and hard to manipulate. Micro-structured fibers are an alternative to common step index optical fibers for evanescent wave sensing where the sample could be flowed inside the hollow core, offering a more robust structure [5]. Although optical fibers offer a long interaction length and are useful for remote sensing, they do not allow for multiplexing. On the other hand, planar waveguides allow for easy fabrication, multiple analyte detection for a unique sample, microfluidic integration, and are structurally more robust than optical fibers. Planar waveguides are usually single mode waveguides where a thin layer of material is deposited on a substrate of lower refractive index, thus acting as the waveguide core. The coupling of light to the waveguide is usually accomplished with a prism or grating, where the incoming light has to be directed to a specific angle for wave vector matching. The components required for light coupling and signal analysis required to fabricate a functional biosensor with planar waveguides make the system quite bulky [6]. Miniaturization and integration of optical and microfluidics components in a single platform is key to develop an integrated optical biosensor that could fit on a chip, hence the name lab-on-a-chip [7]. Rectangular waveguides, are so far the best candidates for this function. Indeed, rectangular waveguides have the advantage to be modeled in different designs and can be matched with more sophisticated integrated optical components for signal processing, such as Bragg filters, spectrophotometers, interferometers, micro resonators, etc. Light coupling can also be facilitated with larger rectangular multimode waveguides by direct coupling. Silicon based materials are the most popular for the fabrication of integrated optics [8] and have also been used for the fabrication of rectangular waveguides in integrated optical evanescent wave sensors [9]–[11]. Although inorganic materials make the most of the integrated optical components, particular properties from polymer materials make them an interesting medium for integrated optics [12]. Their simpler fabrication process and ease of integration over mineral materials make them an attractive choice especially for the optical telecommunication industry [13]. Indeed, polymers can be fabricated with embossing [14] and stamping [15], which offers the possibility for cheap and high volume manufacturing. Other fabrication methods were also used for polymers as direct photolithography [16], laser ablation [17], reactive ion etching (RIE) [18], dip-floating [19], electron-beam writing [20], etc. Also, compared to silica and silicon, polymers have a low thermal conductivity but a high thermo-optic coefficient, which is ideal for thermal actuation [21]. This property allows for high performance thermo-optical devices to be developed [22]–[24]. Another interesting property is that polymeric waveguides have the ability to be flexible. This unique characteristic was justifiably used to develop flexible optical interconnects [25], [26] or strain sensors [27], [28] with polymeric materials. Moreover, polymers were used for optical biosensors as the medium to fabricate different kind of sensing platforms as planar waveguides [29], inverted rib waveguides [30], micro resonators [31], interferometers [32], rectangular waveguides [33], etc. As for bio sensing assays, the analytes contaminate the sensing platform after binding and would alter the response of future examinations. Hence, since polymers are cheap and easy to fabricate, they are ideal for disposable biosensors [34]. A great variety of polymer materials were suitable for integrated optical devices such as acrylates [35], polyimides [36], polycarbonates [37], olefins [38] and epoxide [39]. SU-8, an epoxy based negative photo resist developed in 1989 by IBM, has demonstrated great potential for being a material of choice for integrated optical waveguides due to its transparency to a wide range of wavelengths [16], high resolution [40], mechanical resistance [41], and biocompatibility [42], [43] for bio sensing purposes. For this reason SU-8 will be used in this work as the core material of the waveguides. Various methods have been developed to increase the sensitivity of evanescent wave fluorescent spectroscopy of planar or rectangular waveguide such as, gratings [44], micro cavities [45], surface plasmon-enhanced fluorescence [46], etc. A novel fabrication process for SU-8 waveguides on quartz developed by *Abdul-Hadi et al.* [47] has demonstrated lower optical propagation losses and an increased index of refraction of the SU-8 core, which were exploited to increase the sensitivity of evanescent wave fluorescence spectroscopy.

Our previous work focused on developing polymer waveguides for low optical losses. This paper aims to evaluate the effect of the novel fabrication process for SU-8/quartz waveguide [47] on evanescent fluorescence spectroscopy and to compare it with a SU-8/silica waveguide fabricated

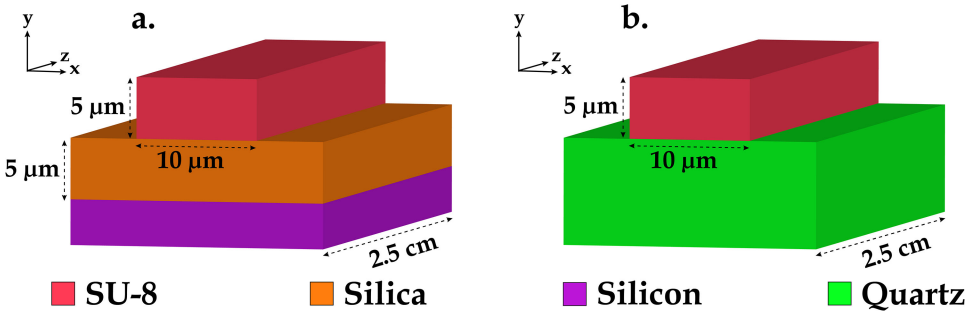

Fig. 1. SU-8 waveguides on (a) silica-on-silicon and (b) quartz substrates.

TABLE 1

Indices of Refractions of the Cores, Substrates, Cladding and Asymmetry Parameters (Along Y Axis) of the SU-8/Quartz and SU-8/Silica Waveguides for a Fluorescence Light Wavelength of $\lambda = 671$ nm

Waveguides	Index of refraction (λ= 671 nm)			Asymmetry parameters	
	Cores	Substrates	Cladding	TE	TM
SU-8/quartz	1.587	1.456	1.330	0.88	1.78
SU-8/silica	1.580	1.459	1.330	0.98	1.94

with the standard protocol. 3D FDTD simulations with randomly oriented and phased dimensionless emitting current dipoles for the SU-8 waveguides on quartz and silica substrates were used to compare the fluorescence coupling of both sensing platforms. Finally, in this work, the SU-8 waveguides on quartz fabricated with our optimized process [47] are compared with SU-8 waveguides on silica fabricated with the standard protocol for evanescent fluorescence spectroscopy with Bovine Serum Albumin labelled with Alexa 647 (BSA-Alexa 647) as the analyte of interest.

2. Design

SU-8 5 photoresist (Microchem, Newton, U.S.A) was the preferred material for the waveguides cores. An oxidized silicon wafer with a 5-μm thick silica layer (Rogue Valley Micro Devices, Medford, U.S.A) and a 1-mm thick fused quartz wafer (Semiconductor Wafer, Hsinchu, Taiwan) were chosen as substrates. The width, the thickness, and the length of the waveguides were 10 μm, 5 μm, and 2.5 cm respectively (Fig. 1(a) and (b)) following the same dimensions as the structures in [47].

The indices of refraction of the SU-8 cores and substrates were previously measured by ellipsometry (also in [47]) and presented in Table 1 for the fluorescence light wavelength ($\lambda = 671$ nm). Water is used as the cladding for the purpose of this work. The asymmetry parameters (along the y axis) [48] were calculated accordingly to the waveguides respective indices of refraction.

The indices of refractions of the cores and substrates of the waveguides for the fluorescence collection efficiency calculations in the remainder of the document are taken from Table 1. The dimensions and indices of refraction for the SU-8/quartz and SU-8/silica configurations allows for highly multimodal waveguides for $\lambda = 671$ nm. With the help of the effective index method it was numerically solved that for $\lambda = 671$ nm the SU-8/quartz and SU-8/silica waveguides allows for approximately 137 and 126 guided (TE or TM) modes respectively.

3. Fabrication and Characterization

The fabrication of the SU-8 waveguides on the silica-on-silicon and quartz substrate was done by way of UV lithography. However, the processes for each substrates differed. The fabrication protocol for the SU-8 waveguides on the silica-on-silicon substrate followed the basic guidelines

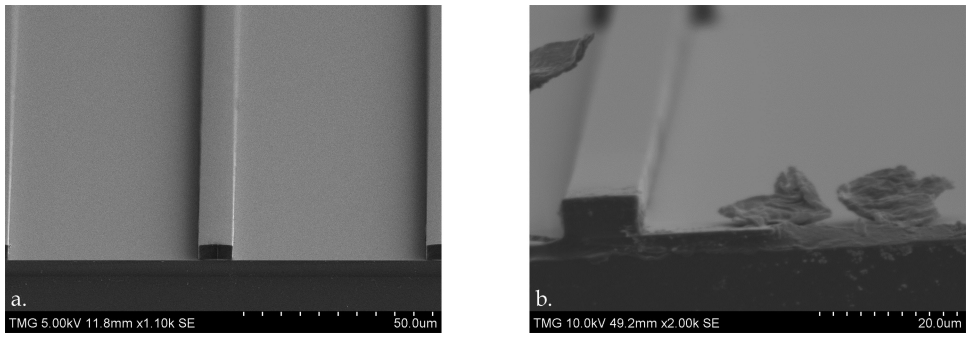

Fig. 2. SEM pictures of the (a) SU-8/silica and (b) SU-8/quartz waveguides.

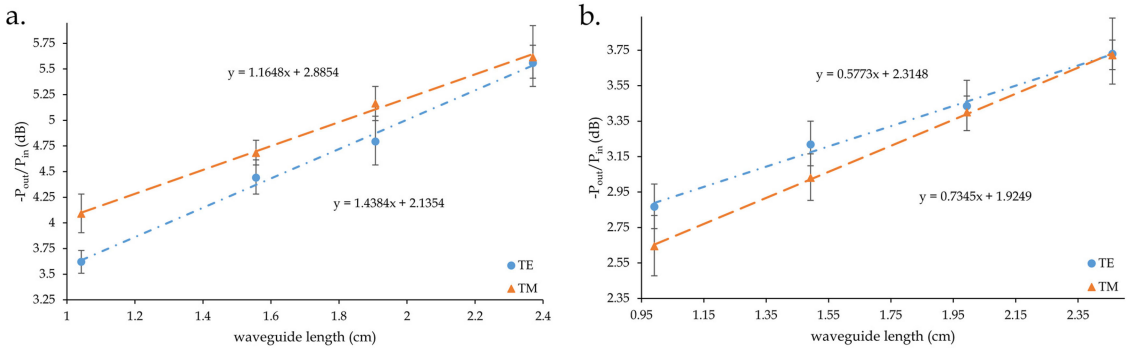

Fig. 3. Optical propagation losses for the TE and TM polarizations evaluated with the cutback method for (a) SU-8/silica and (b) SU-8/quartz waveguides.

of the standard protocol. However, the standard fabrication protocol was not suitable for the SU-8 waveguides on quartz. A comparative study performed by *Abdul-Hadi et al.* [47], gives detailed explanations about the fabrication process of SU-8 waveguides on a silica-on-silicon and quartz substrates and the resulting characteristics of both waveguides. The same fabrication steps used in [47] were used in this work for the fabrication of the SU-8 waveguides on silica-on-silicon and quartz. Scanning electron microscopy (SEM) images of the SU-8/Quartz and SU-8/Silica are shown on Fig. 2.

The most important results from [47] are the lower optical propagation losses of the SU-8/Quartz waveguides compared to the SU-8/Silica waveguides obtained from the optimized fabrication process as shown on Fig. 3.

It is obvious from Fig. 3 that the optical propagation losses for both TE and TM polarizations are lower for the SU-8/quartz waveguide than the SU-8/silica waveguide. A more detailed explanation about the nature of the optical losses is given in [47]. Lower asymmetry parameters (Table 1) and lower optical propagation losses (Fig. 3) could advantage the SU-8/quartz waveguide compared to the SU-8/silica waveguide for evanescent wave fluorescence spectroscopy assays. The remainder of the document will address this claim with the help of 3D FDTD simulations and a evanescent wave fluorescence spectroscopy experiment with different concentrations of BSA labeled with Alexa fluor 647.

4. Theory

4.1 Evanescent Fluorescence Coupling Near a Dielectric Waveguide

A dielectric surface near a radiating dipole, in our case a fluorophore, modifies the angular distribution of the emitted light [49] and at the same time provokes a back-coupling of the fluorescence in the dielectric medium [50]. The light propagating in the dielectric is partly under the critical angle,

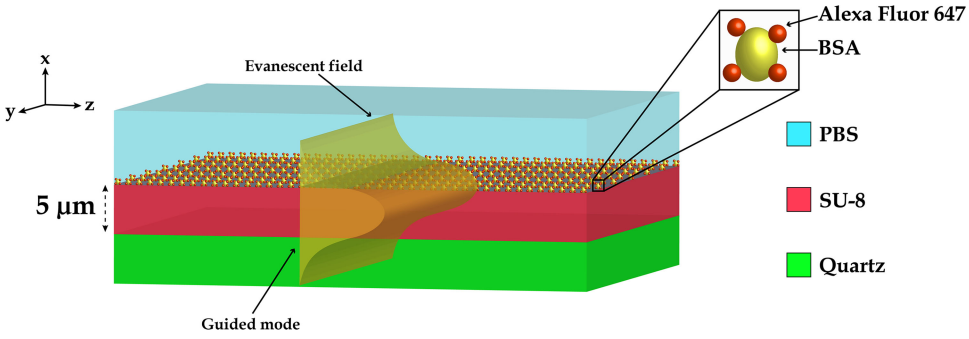

Fig. 4. Schematic representation of the fundamental mode propagating through a planar waveguide with a SU-8 core layer, a PBS cladding, and quartz substrate with BSA-Alexa 647 immobilized on the SU-8 surface.

termed 'allowed' light [51], and partly above the critical angle, termed 'forbidden' light [51]. The light propagating above the critical angle, can be guided if another layer is added as a substrate if its index of refraction is lower than the dielectric layer, understanding that the dipole is also located in a medium of lower index than the dielectric layer. This arrangement is called a waveguide (Fig. 4), where the dielectric layer is acting as the guiding layer for the light. In this work, the fluorophores are attached to a BSA protein and diluted in a buffer solution (PBS). The buffer solution is mainly composed of water, hence its index of refraction is around 1.33. Alexa Fluor 647 was chosen as the fluorescent dye which can be excited with a 635 nm light and has a peak emission at a wavelength of around $\lambda = 671$ nm. The BSA molecule, in this work, can be seen as a prolate ellipsoid with diameters of 14 nm and 4 nm of size [52] with a labeling degree of 4. Therefore, the distance between the fluorophore and the PBS-SU-8 interface is approximated to be 10 nm. The light in the forbidden region is guided through, for instance, the SU-8/quartz waveguide formed by the buffer solution, the SU-8 core and the quartz substrate, Fig. 4. It has been demonstrated that when a fluorophore is excited near a higher refractive index medium it emits evanescent waves that are transformed into propagating plane waves by the medium [50].

The emission of the fluorophore couples to the evanescent field of the guided mode(s) (Fig. 4). This phenomenon is called evanescent coupling and is used to detect labeled biological entities immobilized on the waveguide by measuring the guided fluorescence light at the output of the waveguide.

The fluorescence collection efficiency gives the proportion of the light from the sources captured and guided by the waveguide. A more extensive definition of the fluorescence collection efficiency can be found in [53], [54]. Although, in this work, the waveguides are rectangular in shape the same principle applies for the fluorescence evanescent coupling but the modes will be confined in a 2D geometry instead. The calculation of the fluorescence collection efficiency for sources near a planar dielectric planar waveguide was already developed by Srivastava *et al.* [54] with the modal propagation approach. However, to calculate the fluorescence collection efficiency with the modal propagation approach for rectangular waveguides will require the use of the effective index method. The effective index method works better for high width/thickness ratio and low index contrast. Since the dimensions of the SU-8/quartz and SU-8/silica waveguides are 10×5 μm and the index contrast is moderately high. A relative study may be acceptable using this method, but for a more accurate calculation the FDTD method would be more appropriate.

5. 3D FDTD Modeling of Simulated Fluorophores in the Vicinity of the SU-8/Quartz and SU-8/Silica Waveguides

The 3D FDTD numerical method was used for an accurate evaluation of the relative difference of the fluorescence collection efficiencies between the waveguides with a 10-nm Alexa-647 fluorescent

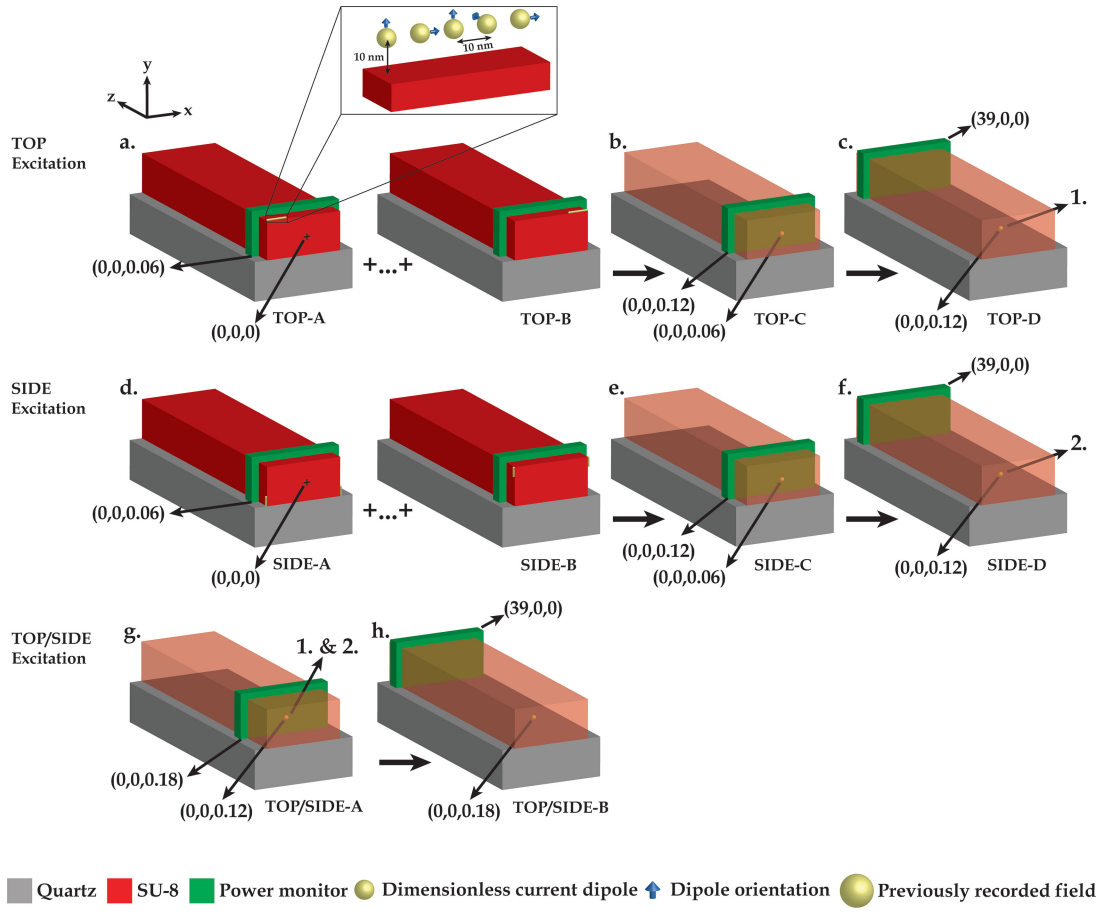

Fig. 5. Successive steps for the 3D FDTD simulation of a line(s) of dimensionless, randomly oriented and phased emitting current dipoles on the (a) top, (d) sides and (g) combined fields of the top and sides of a SU-8/quartz or SU-8 silica waveguide for the evaluation of the guided coupled light propagating through the waveguide.

layer located on the top or on the sides of the waveguides. Firstly, a study with a 3D FDTD model of the SU-8/quartz and SU-8/silica waveguides with simulated fluorophores close to the waveguide surface was performed to evaluate the collection efficiency at the output of the waveguide. Emitting dimensionless dipoles were used to simulate the Alexa-647 fluorophores. As mentioned above, the BSA molecule was approximated to a size of 10 nm. The dipoles were then located at a 10 nm distance from the waveguides and also spaced from one another at a distance of 10 nm. The simulated fluorophores were uniformly distributed from one extremity to the other for the top and side part of the waveguides. The simulation was performed with the FDTD software *Fullwave* from *Synopsis*. Covering with simulated fluorophores from the left extremity to the right extremity along the top and from bottom to the top for the sides of the waveguide would require 1001 and 1002 simulated fluorophores respectively, if spaced from one another at a distance of 10 nm. That amount of simulated fluorophores exceeded the limits of the software. Only 32 simulated fluorophores are allowed at once. A series of simulations with each simulation having the maximum number of simulated fluorophores was performed until fully covering a 10 μm line along the top or two 5 μm lines on the sides of the waveguides. For each simulation, the monitor was placed at 60 nm from the fluorophores and the resulting field was recorded (Fig. 5(a), (d)). Each of the successive resulting fields from each simulation were then combined as a single source (Fig. 5(b), (e)). The simulation of this source was then performed and the resulting field was also recorded at a distance of 60 nm

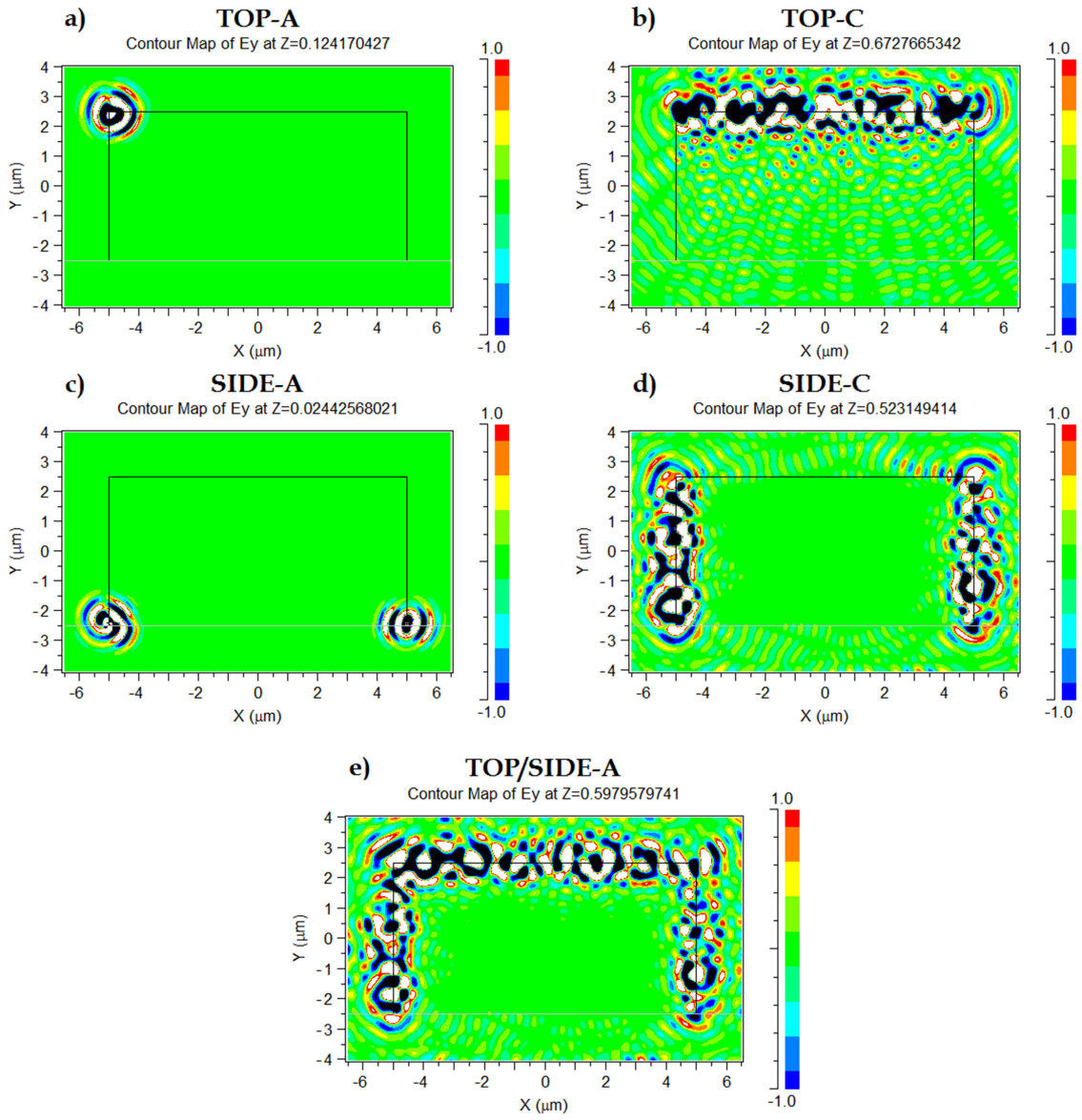

Fig. 6. Total electric field E_y for 32 emitting dimensionless, randomly oriented and phased current dipoles (a) on the top left and (c) both sides (2×16) of the SU-8/quartz or SU-8/silica waveguide facets. Total resulting field E_y from the emitted light from 1001,1002 and 2003 simulated fluorophores on the (b) top, (d) sides (2×501) and (e) top/sides of a 10×5 μm SU-8/quartz or SU-8/silica waveguide.

(Fig. 5(b), (e)). The last simulation was then performed, for which the resulting field propagated along the remainder of the 39 μm long waveguide (Fig. 5(c), (f)). The resulting fields from the top and sides of the waveguides were combined and the resulting field was recorded at 60 nm from it's initial position (120 nm; Fig. 5(g)). A monitor was placed at 39 μm distance from the start of the waveguide to measure the averaged power at the output (Fig. 5(c), (f), (h)). The ratio between the measured averaged power between the SU-8/quartz and SU-8/silica waveguides gives the increase in fluorescence collection efficiency between both waveguides. The dipoles were randomly oriented only along the x, y or z axis as depicted on the inset of Fig. 5. Also, the phase of each dipole was randomly generated from 0° to 360°.

TABLE 2
Average Values of the Ratios of the Fluorescence Collection Efficiencies (F.C.E) for the Different Distributions of Randomly Oriented and Phased Dimensionless Current Dipoles for the Top, Sides and Top/Sides Between the SU-8/Quartz and SU-8/Silica Waveguides

		Distribution number	SU-8/Quartz	SU-8/Silica	F.C.E Ratio (%)	Average of F.C.E ratios (%)	Standard deviation (%)
Fluorescence Collection efficiency	Top	1	4.04	3.64	10.88	10.3	1.2
		2	3.01	2.71	11.11		
		3	4.42	4.07	8.48		
		4	3.20	2.90	10.51		
	Side	1	5.92	5.72	3.44	3.4	1.3
		2	6.86	6.52	5.14		
		3	7.97	7.74	2.95		
		4	7.51	7.36	2.08		
	Top/Side	1	3.98	3.74	6.32	5.4	1.4
		2	3.64	3.41	6.54		
		3	4.98	4.73	5.30		
		4	4.20	4.06	3.42		

The total electric field E_y, with a view from the waveguide facet, is shown on Fig. 6(a), (c) for a simulation of 32 simultaneously emitting dimensionless dipoles at the top and sides of the waveguide. The results of the simulations in Fig. 6(a), (c) displays the electric field emissions from the configurations (1st image) of Fig. 5(a), (d) respectively. The combined fields of the series of simulations resulting in 1001 (top),1002 (2 x 501) (sides) and 2003 (top/sides) emitting dipoles are shown on Fig. 6(b), (d), (e). The results of the simulations in Fig. 6(b), (d), (e) displays the electric field emissions from the configurations of Fig. 5(b), (e), (g) respectively. The ratios between the averaged powers from four different distributions of randomly oriented dipoles and phases for the top, sides and top/sides of the of SU-8/quartz and SU-8/silica waveguides are shown on Table 2.

It is seen from results from Table 2 that the SU-8/quartz waveguide presents a higher fluorescence collection efficiency than the SU-8/silica waveguide for any sides of the waveguides. If the rectangular waveguide is approximated as 2 planar waveguides, the planar waveguide varying in index along the y axis will have a TE/TM asymmetry parameters [55] of 0.88/1.78 for SU-8/quartz waveguide and 0.98/1.94 for SU-8/silica waveguide. The asymmetry parameters of the planar waveguides varying in index along the x axis will be nil. It was shown in [54] that a lower asymmetry increases the fluorescence collection efficiency. Hence, the higher collection efficiency from the top of the waveguide. Although, the asymmetry parameters are nil for the sides of the waveguides, the core index of the SU-8/quartz waveguide is higher than the core of the SU-8/silica waveguide. It was also shown from [56] that a higher index core increases the fluorescence collection efficiency. Indeed, a higher core index increases the coupling of the light of the emitting fluorophores by increasing the confinement of the light near the core cladding interface. While a higher substrate index will drag more of the power of the modes in the substrate resulting in less power in the cladding, resulting in lower fluorescence collection efficiency. The SU-8/quartz waveguide fabricated with the novel process from [47] have both a higher core index and a lower substrate index than the SU-8/silica making it a better choice for evanescent fluorescence spectroscopy.

6. Fluorescence Evanescent Wave Spectroscopy

6.1 Experimental Setup

The experimental setup used for the detection of the Alexa-647 labeled BSA by fluorescence evanescent wave spectroscopy is illustrated on Fig. 7. The excitation light source used was a fiber-coupled laser diode with a 635 nm central wavelength (OZ optics, Westbrook, Canada). A

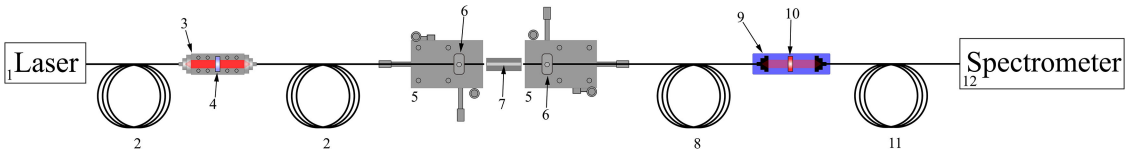

Fig. 7. Fluorescence evanescent wave spectroscopy experimental setup. 1) Fiber-coupled laser ($\lambda = 635$ nm). 2) Single mode fiber. 3) Single mode fiber-to-fiber coupler. 4) 650 nm shortpass filter. 5) Five-axis stage micro positioners. 6) Fiber holders. 7) SU-8/quartz or SU-8/silica waveguide. 8) Mutlimode fiber (62,5 μm core). 9) Multimode fiber-to-fiber coupler. 10) 676-29 nm bandpass filter. 11) Multimode fiber (600 μm core). 12) Spectrometer.

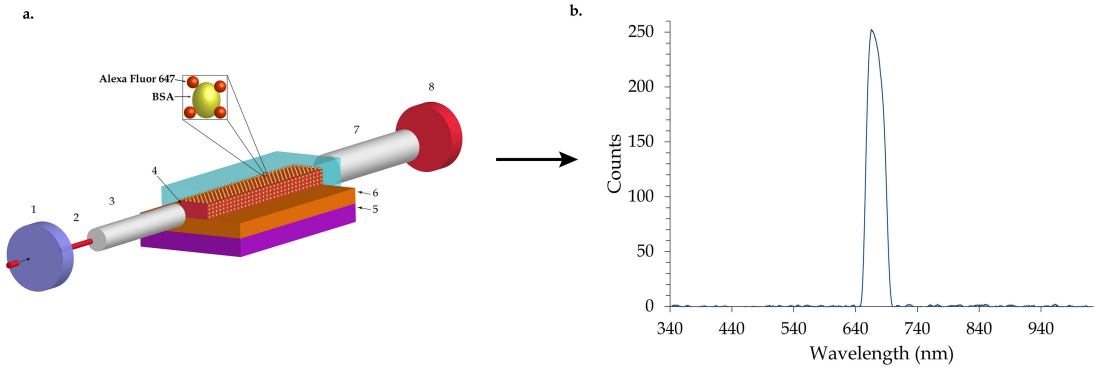

Fig. 8. Arrangements of the SU-8/silica waveguide with the immobilized BSA-Alexa 647 (a) with the 650 nm shortpass filter and the 676/29 nm bandpass filter, (b) the resulting spectrum. The components on a) are 1) 650 nm shortpass filter, 2) laser ($\lambda = 635$ *nm*), 3) single mode fiber, 4) SU-8 core, 5) silicon wafer, 6) silica substrate, 7) multimode fiber, 8) 676/29 nm bandpass filter.

single mode fiber with a 3.6-5 μm mode field diameter (Thorlabs, Newton, USA) was connected to the fiber-coupled laser diode and to the input of a single mode fiber coupler (Thorlabs, Newton, USA) containing a 650 nm shortpass filter (Thorlabs, Newton, USA). This light source was butt-coupled to the input of the SU-8/quartz or SU-8/silica waveguide. The excitation light guided through the waveguide was collected simultaneously with the guided fluorescence light coupled to the waveguide from the BSA-Alexa-647 by a 62.5 μm core multimode fiber (Thorlabs, Newton, USA) at the output of the waveguide. The 62.5 μm core multimode fiber was also connected to a multimode fiber coupler (Ocean Optics, Largo, USA) holding a 676/29 nm bandpass filter (Semrock, Rochester, USA). Finally, the light was guided through a 600 μm multimode fiber (Ocean Optics, Largo, USA) to a spectrometer (USB-2000 Ocean optics) to be spectrally analyzed.

The two interference filters were essential to discriminate the guided fluorescence light from the Alexa-647 fluorophores. The 676/29 nm bandpass filter (Fig. 8(a)-8) was mainly used to prevent the stray light from the excitation source (635 nm) from entering the spectrometer. Indeed, without any filters, the stray light caused the excitation of pixels that are not attributed to the specific wavelength diffracted by the grating. Therefore, the spectrum was saturated and the fluorescence signal indiscernible. Even only with the 676/29 nm bandpass filter (Fig. 8(a)-8), the fluorescence signal was not discernible from the spectrum. Hence the addition of a 650 nm shortpass filter (Fig. 8(a)-1), to the 676/29 nm bandpass filter (Fig. 8(a)-8), which will let through the excitation light (635 nm) but block the light with a higher wavelength than 650 nm to allow the fluorescence light ($\sim$671 nm peak) to be apparent (Fig. 8(b)). The polarization of the light at the output of the input fiber (Fig. 8-3), was measured to be 41° from the plane of the substrate surface.

6.2 SU-8 Autofluorescence

It was already shown that SU-8 shows a strong fluorescence at visible wavelengths [57]. Bleaching of the SU-8 autofluorescence can be achieved with a long illumination [58]. Before proceeding with

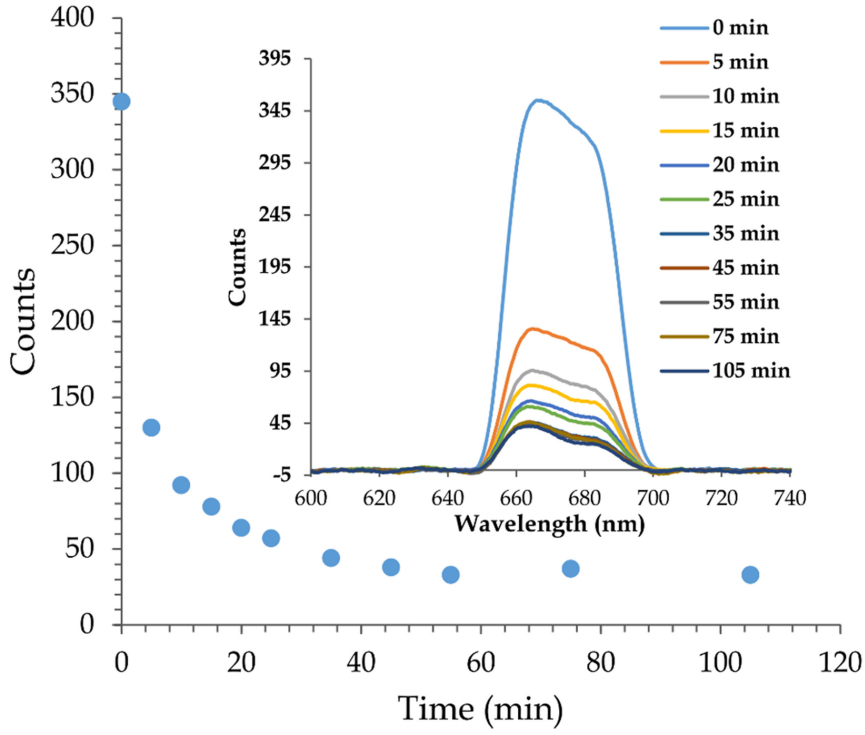

Fig. 9. Intensity (counts) of the SU-8 autofluorescence in function of time from a 635 nm laser light guided through the SU-8 core of a SU-8/silica waveguide. Inset: spectra of the SU-8 autofluorescence signals (after smoothing).

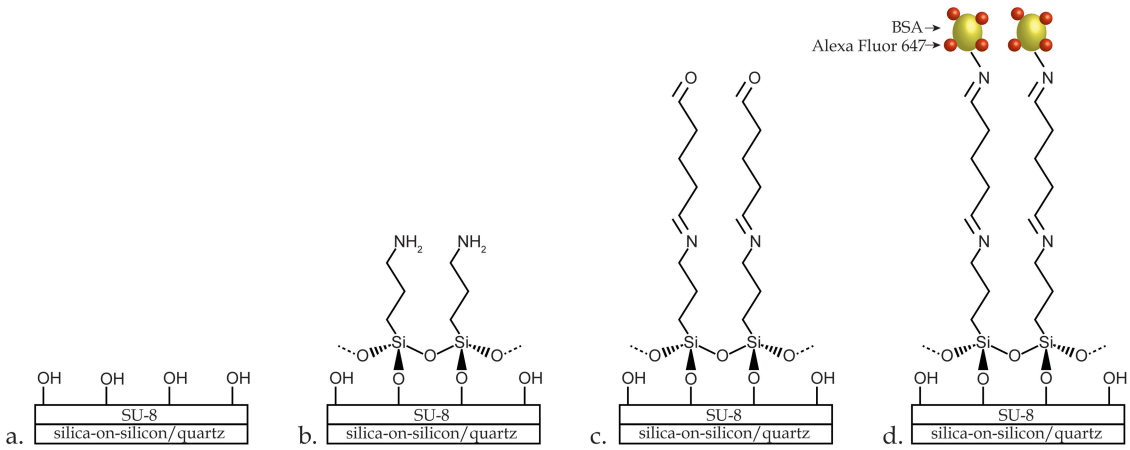

Fig. 10. Schematic of the immobilization steps. (a) Functionalization. (b) Silanization. (c) Glutaraldehyde treatment. (d) BSA-Alexa 647 immobilization.

the evanescent wave spectroscopy, a complete photobleaching of the SU-8 waveguides was done to get rid of the fluorescence background with the help of the 1 mW laser light ($\lambda = 635\ nm$) guided through the waveguide. The spectrum of the output signal of a SU-8 waveguide on a silica-on-silicon substrate was taken at different time, Fig. 9, with continuous illumination until no change was visible in the intensity of the spectrum.

The photobleaching of the SU-8 cores for both the SU-8/silica and SU-8/quartz waveguides was complete after around 55 min of illumination, Fig. 9. Fading of the fluorescence was permanent. Indeed, the photobleaching was effective even weeks after the illumination session.

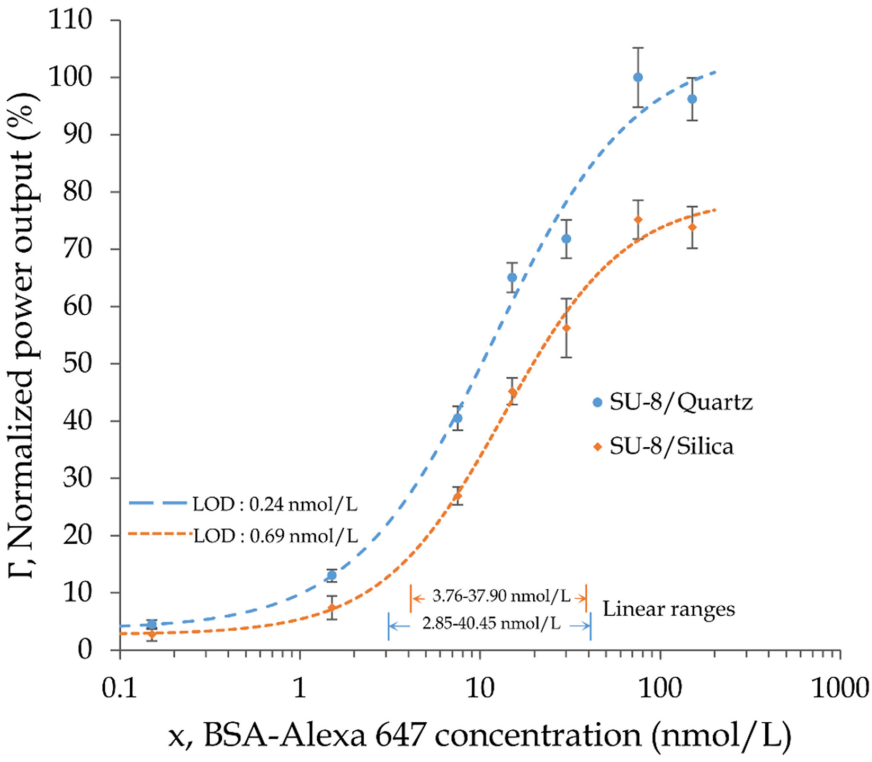

Fig. 11. Calibration curves for the fluorescence evanescent spectroscopy of BSA-Alexa 647 fluor immobilized on SU-8/Quartz and SU-8/Silica waveguides.

6.3 Immobilization of BSA-Alexa 647 on SU-8/Quartz and SU-8/Silica Waveguides

The immobilization procedures were identical for both SU-8 waveguides on silica-on-silicon and quartz substrates. Firstly, the chips were rinsed with acetone and isopropanol. After drying with a nitrogen jet, the chips were exposed to oxygen plasma for 20 seconds to functionalize the surface with OH groups (Fig. 10(a)). After, the chips were silanized by immediate immersion in 1% (v/v) APTES-ethanol solution for 1 hour at room temperature (Fig. 10(b)). The chips were then rinsed with ethanol and DI water, dried with a gentle nitrogen flow and kept in oven at 100°C for 10 min. After cooling down to room temperature, drops of 1, 2% (v/v) glutaraldehyde-PBS (glutaraldehyde-Phosphate buffered saline) solution were placed on the SU-8 waveguides until the entire waveguide was submerged by the solution (Fig. 10(c)), and kept at room temperature for 2 hours in a sealed petri box with a water-soaked paper to prevent the drying of the solution. The waveguide was then flushed with PBS and DI water. After drying with a nitrogen jet, the SU-8 waveguides were exposed to different concentrations of ready-to-use Alexa 647 labeled BSA (Thermofisher Scientific) with PBS as solvent (Fig. 10(d)). The chips were kept at room temperature in a sealed petri box with a water soaked tissue overnight. The waveguide was finally rinsed with PBS and was always kept wet (with PBS over the entire length of the waveguides).

6.4 Fluorescence Detection From BSA-Alexa 647 Immobilization

After complete photobleaching of the SU-8 cores for both the SU-8/silica and SU-8/quartz waveguides, a comparative study was performed to evaluate the fluorescence output of each waveguide with different concentrations of BSA-Alexa 647 immobilized following the steps on Fig. 10. All the waveguides were cleaved so that they were 2.5 cm long. The cleaving techniques were similar to those described in [47], i.e., scratching the edge of the silica-on-silicon wafer and applying pressure on both sides of the scratch to obtain a sharp fissure. For the SU-8/quartz waveguide, the quartz

wafer was diced from the back while leaving 50 μm of material and cleaved by applying pressure on both sides of the dicing line.

Fluorescence evanescent spectroscopy was performed with concentrations of BSA-Alexa 647 varying from 0.15 nmol/L to 15 nmol/L. The responses of the waveguides are expressed as the normalized fluorescence power output, Γ, which is defined as $\Gamma = \frac{P^*_{wg}}{P^*_{wg}max}$ with P^*_{wg} referring to P_{wg} from [54], but including optical losses and $P^*_{wg}max$ the measured fluorescence output for SU-8/Quartz at saturation (75.20 nmol/L). Since the experiment is a ligand binding assay, the experimental data for the SU-8/quartz and SU-8/silica waveguides were fitted with the commonly used 4 parameters logistic regression model [59]:

$$Y = D + \frac{(A - D)}{\left(1 + \left(\frac{x}{C}\right)^B\right)} \tag{1}$$

Where Y is the response, A the lower asymptote, D the upper asymptote, B the slope factor, C the analyte concentration at the inflection point of the calibration curve, and x the analyte concentration. This led to the following equations: $\Gamma = ((3.68 - 105.20)/1 + (\frac{x}{11.96})^{1.106}) + 105.20,\ R^2 = 0.9889$ and $= ((2.73 - 79.22)/1 + (\frac{x}{13.46})^{1.275}) + 79.22,\ R^2 = 0.9953$. The linear dynamic ranges for each waveguides were evaluated as an interval going from 20% to 80% of the value of $D - A$ [60]. The linear ranges corresponds then to 2.85–40.45 nmol/L and 3.76–37.90 nmol/L for SU-8/Quartz and SU-8/Silica waveguides respectively. The linear regression equations were adjusted to $\Gamma = 25.92 \ln x - 9.63, \quad R^2 = 0.9985$ and $\Gamma = 22.15 \ln x - 16.45, \quad R^2 = 0.9982$. The limits of detection were determined as the analyte concentrations at the blank$+ 3\sigma$ (where σ is the standard deviation of the blank signal) [61], which were 0.24 and 0.69 nmol/L for SU-8/Quartz and SU-8/Silica waveguides, respectively.

7. Discussion

Many parameters can affect the fluorescence evanescent coupling spectroscopy between the SU-8/Quartz and SU-8/Silica waveguides. The dimensions of the waveguides can be affected by the fabrication process. As shown from [47], the width of the SU-8/Quartz waveguide ($\sim$10 μm) is around 10% greater than the SU-8/Silica waveguide ($\sim$9 μm) due to the different fabrication protocols. Although the fluorescence collection efficiency is not affected by the width difference for highly multimode waveguide [56], the larger width offers a greater area that would accommodate more labeled analyte leading to a higher fluorescence coupling. This characteristic will result in an increase in the fluorescence light output that should be taken into account when comparing the calibration curves of both waveguides. The thicknesses of the waveguides should not affect the fluorescence output since they are similar, as seen in [47]. It was seen from the calibration curves, Fig. 11, that the sensitivity of the SU-8/Quartz waveguides was greater than the SU-8/silica waveguides. The enhancement in sensitivity can be determined by the ratio of the slope of the linear regression equations, which gives 17% enhancement in sensitivity. Also, the limits of detection were evaluated as the analyte concentrations of the blank signal $+ 3\sigma$ (where σ is the standard deviation of the blank signal) [61], which were 0.24 and 0.69 nmol/L for the SU-8/Quartz and SU-8/Silica waveguides, respectively. As explained above, the lower asymmetry and optical losses due to the choice of substrates and the particularities of the fabrication processes that led to different indices of refraction resulted in a greater fluorescence evanescent coupling and less optical losses from the guided fluorescence light. This led to a higher fluorescence output for the SU-8/Quartz waveguide for a similar labeled analyte concentration. Although the linear ranges should be similar since the immobilization protocols were similar for both waveguides, the small difference observed in the linear ranges of both waveguides was probably due to experimental errors. According to [47], the optical propagation losses, for both waveguides, determined for the TE polarization, differed from the ones evaluated with the TM polarization. Taking this into consideration, and the fact that the light polarization at the input of the waveguides was measured to be 41° from the plane of the substrate surface,

the guided light output should be 48% higher for the SU-8/quartz waveguide by calculating the optical losses for both waveguides with the values from Fig. 3 with respect to the measured input light polarization. Also, from the 3D FDTD simulations the average value of the ratio of the 4 distributions (with randomly phased and oriented simulated fluorophores) for the total fluorescence collection efficiency for both waveguides was evaluated to be 5.39 $\pm$ 1.42% (error = standard deviation), Table 2.

Taking into consideration the values from above, the fluorescence light output for the SU-8/Quartz waveguides should be around 63% greater than the SU-8/silica waveguides if, as mentioned above, 10% of its surface is larger, it's lower asymmetry contribute to 5.4 $\pm$ 1.4% (Table 2) increase, and the optical propagation losses are 48% lower. For comparison, the average of the ratios of the averaged values of the relative signal (%) (Fig. 11) between both waveguides gives an average fluorescence output enhancement of 46 $\pm$ 18% (error = standard deviation). In brief, the lower asymmetry parameters (Table 1) of the SU-8/quartz waveguide compared to the SU-8/silica waveguide contribute to a higher fluorescence output of 5.4 $\pm$ 1.4% as demonstrated by the 3D FDTD simulations. Also, if the asymmetry contribution for the fluorescence output is about 5.4 $\pm$ 1.4% and the average fluorescence output enhancement is 46 $\pm$ 18% it could be understood that the enhancement from the lower optical propagation losses of the SU-8/quartz waveguide (Fig. 3) should be of 41 $\pm$ 18% or 31 $\pm$ 18% taking into account the 10% greater area of the SU-8/quartz waveguide. Interestingly, it is the first time that fluorescence spectroscopy was done with direct coupling on a SU-8 on quartz rectangular waveguide. The SU-8 core and quartz substrate being both transparent to visible light could offer the possibility to perform fluorescence microscopy from the bottom of the substrate at the same time than fluorescence spectroscopy. This could be convenient if microfluidics are bonded on the top of the chip. Also, the fabrication process used for the SU-8/quartz waveguide [47] conveniently increases the core index of refraction and smoothes the side walls of the waveguide, which is favorable for evanescent wave fluorescence spectroscopy as shown is this work. This fabrication process could also be applied to other photo resist materials for rectangular waveguides for evanescent wave fluorescence spectroscopy. That being said, the fabrication process could be greatly improved if other parameters, such as temperature and humidity were controlled. These parameters could particularly influence the solvent concentration within the photo resist during the long soft bake specific to the SU-8/quartz waveguide fabrication process which is a crucial factor to obtain smoother waveguide walls as stated in [47]. Therefore it could modify the optical propagation losses from time to time. Hence, also the guided fluorescence light output.

8. Conclusion

A comparative study was done to evaluate the performance of a SU-8 rectangular waveguide on a quartz substrate fabricated with a novel process with a SU-8 waveguide on a silica-on-silicon substrate fabricated with the standard protocol for fluorescence evanescent spectroscopy. A 3D FDTD analysis was performed to evaluate the difference between the fluorescence collection efficiencies between both waveguides by simulating randomly oriented and phased dimensionless current dipoles acting as fluorophores along the top and sides of the waveguides. Fluorescence evanescent wave spectroscopy with different concentrations of BSA-Alexa 647 was experimented on the SU-8/Quartz and SU-8/silica waveguides. The fluorescence biodetection calibration curves revealed that the SU-8/Quartz waveguides showed a 17% enhancement in sensitivity compared to the SU-8/Silica waveguide fabricated with the standard protocol. Also, the limits of detection went as low as 0.24 nmol/L and 0.69 nmol/L for the SU-8/Quartz and SU-8/Silica waveguides respectively. A higher sensitivity could probably be attained if control over the temperature and humidity was available during the fabrication processes. An optimization of these parameters could results in smoother waveguide sidewalls. Also, the 3D FDTD analysis to evaluate the fluorescence collection efficiency for fluorophores in the vicinity of a rectangular waveguide could be extended to different fluorophores and rectangular waveguides with different dimensions and indices of refraction.

References

[1] C. McDonagh, C. S. Burke, and B. D. MacCraith, "Optical chemical sensors," *Chem. Rev.*, vol. 108, no. 2, pp. 400–422, Feb. 1, 2008.
[2] C. R. Taitt, G. P. Anderson, and F. S. Ligler, "Evanescent wave fluorescence biosensors," *Biosensors Bioelectron.*, vol. 20, no. 12, pp. 2470–2487, Jun. 15, 2005.
[3] M. Pospíšilová, G. Kuncová, and J. Trögl, "Fiber-optic chemical sensors and fiber-optic bio-sensors," *Sensors*, vol. 15, no. 10, pp. 25208–2529, 2015.
[4] A. Leung, P. M. Shankar, and R. Mutharasan, "A review of fiber-optic biosensors," *Sensors Actuators B, Chem.*, vol. 125, no. 2, pp. 688–703, 8/8/2007.
[5] E. P. Schartner *et al.*, "Taming the light in microstructured optical fibers for sensing," *Int. J. Appl. Glass Sci.*, vol. 6, no. 3, pp. 229–239, 2015.
[6] K. E Sapsford *et al.*, Fluorescence-based array biosensors for detection of biohazards," *J. Appl. Microbiol.*, vol. 96, pp. 47–58, 2004.
[7] M. C. Estevez, M. Alvarez, and L. M. Lechuga, "Integrated optical devices for lab-on-a-chip biosensing applications," *Laser Photon. Rev.*, vol. 6, no. 4, pp. 463–487, 2012.
[8] T. David *et al.*, "Roadmap on silicon photonics," *J. Opt.*, vol. 18, no. 7, p. 073003, 2016.
[9] A. Fernández Gavela, D. Grajales García, J. C. Ramirez, and L. M. Lechuga, "Last advances in silicon-based optical biosensors," *Sensors*, vol. 16, no. 3, p. 285, Feb. 18, 2016.
[10] A. Densmore *et al.*, "A silicon-on-insulator photonic wire based evanescent field sensor," *IEEE Photon. Technol. Lett.*, vol. 18, no. 23, pp. 2520–2522, Dec. 2006.
[11] K. D. Vos, I. Bartolozzi, E. Schacht, P. Bienstman, and R. Baets, "Silicon-on-Insulator microring resonator for sensitive and label-free biosensing," *Opt. Exp.*, vol. 15, no. 12, pp. 7610–7615, Jun. 11, 2007.
[12] L. Eldada and L. W. Shacklette, "Advances in polymer integrated optics," (in English), *IEEE J. Sel. Topics Quantum Electron.*, vol. 6, no. 1, pp. 54–68, Jan./Feb. 2000.
[13] L. Kurt, "Optical polymers for telecom applications," *Macromol. Symposia*, vol. 100, no. 1, pp. 65–69, 1995.
[14] R. Bruck *et al.*, "Flexible thin-film polymer waveguides fabricated in an industrial roll-to-roll process," *Appl. Opt.*, vol. 52, pp. 4510–4514, 2013.
[15] K. Junya, Y. Shogo, H. Yutaka, and K. Naomi, "Low loss polymer optical waveguide replicated from flexible film stamp made of polymeric material," *Japanese J. Appl. Phys.*, vol. 52, no. 7R, p. 072501, 2013.
[16] K. K. Tung, W. H. Wong, and E. Y. B. Pun, "Polymeric optical waveguides using direct ultraviolet photolithography process," *Appl. Phys. A*, vol. 80, no. 3, pp. 621–626, Feb. 01, 2005.
[17] S. S. Zakariyah, P. P. Conway, D. A. Hutt, K. Wang, and D. R. Selviah, "CO2 laser micromachining of optical waveguides for interconnection on circuit boards," *Opt. Lasers Eng.*, vol. 50, no. 12, pp. 1752–1756, Dec. 2012.
[18] K. Jae-Wook, K. Joon-Sung, and K. Jang-Joo, "Optimized oxygen plasma etching of polycarbonate for low-loss optical waveguide fabrication," *Japanese J. Appl. Phys.*, vol. 40, no. 5R, p. 3215, 2001.
[19] H. Robert, C. P. Henrik, S. Nina, S. Christer, and B. L. Niels, "Fabrication of reverse symmetry polymer waveguide sensor chips on nanoporous substrates using dip-floating," *J. Micromech. Microeng.*, vol. 15, no. 6, p. 1260, 2005.
[20] W. H. Wong, J. Zhou, and E. Y. B. Pun, "Low-loss polymeric optical waveguides using electron-beam direct writing," *Appl. Phys. Lett.*, vol. 78, no. 15, pp. 2110–2112, 2001.
[21] H. Ma, A. K. Y. Jen, and L. R. Dalton, "Polymer-based optical waveguides: Materials, processing, and devices," *Adv. Mater.*, vol. 14, no. 19, pp. 1339–1365, 2002.
[22] Y. Sun *et al.*, "Polymer thermal optical switch for a flexible photonic circuit," *Appl. Opt.*, vol. 57, no. 1, pp. 14–17, Jan. 2018.
[23] S.-Q. Sun *et al.*, "Design and fabrication of all-polymer thermo-optic variable optical attenuator with low power consumption," *Appl. Phys. A*, vol. 123, no. 10, p. 646, Sep. 18, 2017.
[24] A. M. Al-Hetar, A. B. Mohammad, A. S. M. Supa'at, and Z. A. Shamsan, "MMI-MZI polymer thermo-optic switch with a high refractive index contrast," *J. Lightw. Technol.*, vol. 29, no. 2, pp. 171–178, Jan. 15, 2011.
[25] R. Dangel *et al.*, "Development of versatile polymer waveguide flex technology for use in optical interconnects," *J. Lightw. Technol.*, vol. 31, no. 24, pp. 3915–3926, Dec. 15, 2013.
[26] L. Li *et al.*, "A fully-integrated flexible photonic platform for chip-to-chip optical interconnects," *J. Lightw. Technol.*, vol. 31, no. 24, pp. 4080–4086, Dec. 2013.
[27] X. Gan, H. Clevenson, and D. Englund, "Polymer photonic crystal nanocavity for precision strain sensing," *ACS Photon.*, vol. 4, no. 7, pp. 1591–1594, Jul. 19, 2017.
[28] M. Rosenberger, W. Eisenbeil, B. Schmauss, and R. Hellmann, "Simultaneous 2D strain sensing using polymer planar Bragg gratings," *Sensors*, vol. 15, no. 2, pp. 4264–4272, Feb. 2015.
[29] P. I. Okagbare, J. M. Emory, P. Datta, J. Goettert, and S. A. Soper, "Fabrication of a cyclic olefin copolymer planar waveguide embedded in a multi-channel poly(methyl methacrylate) fluidic chip for evanescence excitation," *Lab Chip*, vol. 10, no. 1, pp. 66–73, Nov. 4, 2010.
[30] J. W. Kim, K. J. Kim, J. A. Yi, and M. C. Oh, "Polymer waveguide label-free biosensors with enhanced sensitivity by incorporating low-refractive-index polymers," *IEEE J. Sel. Topics Quantum Electron.*, vol. 16, no. 4, pp. 973–980, Jul./Aug. 2010.
[31] M. Mancuso, J. M. Goddard, and D. Erickson, "Nanoporous polymer ring resonators for biosensing," *Opt. Exp.*, vol. 20, no. 1, pp. 245–255, Oct. 2012.
[32] J. C. Ramirez, L. M. Lechuga, L. H. Gabrielli, and H. E. Hernandez-Figueroa, "Study of a low-cost trimodal polymer waveguide for interferometric optical biosensors," *Opt. Exp.*, vol. 23, no. 9, pp. 11985–11994, May 4, 2015.
[33] L. Jiang, K. P. Gerhardt, B. Myer, Y. Zohar, and S. Pau, "Evanescent-wave spectroscopy using an SU-8 waveguide for rapid quantitative detection of biomolecules," *J. Microelectromech. Syst.*, vol. 17, no. 6, pp. 1495–1500, 2008.

[34] S. Aikio *et al.*, "Disposable (bio)chemical integrated optical waveguide sensors implemented on roll-to-roll produced platforms," *RSC Adv.*, vol. 6, no. 56, pp. 50414–50422, 2016, doi: 10.1039/C6RA07320D.
[35] C. S. Kuang, W. Y. Yee, and S. Shaari, "Optimized curing process for perfluorinated acrylic polymer optical waveguide," *Sci. Technol. Adv. Mater.*, vol. 6, no. 3, pp. 383–387, Apr. 1, 2005.
[36] S. Tsuyoshi, "Fluorinated polyimide waveguide fabricated using replication process with antisticking layer," *Japanese J. Appl. Phys.*, vol. 41, no. 3R, p. 1379, 2002.
[37] Z. Cai *et al.*, "Novel fluorinated polycarbonate negative-type photoresists for thermo-optic waveguide gate switch arrays," *J. Mater. Chem. C*, vol. 4, no. 3, pp. 533–540, 2016, doi: 10.1039/C5TC03657G.
[38] H. Shug-June and Y. Hsin Her, "Novel cyclo olefin copolymer used as waveguide film," *Japanese J. Appl. Phys.*, vol. 44, no. 4S, p. 2541, 2005.
[39] K. Enbutsu, M. Hikita, S. Tomaru, M. Usui, S. Imamura, and T. Maruno, "Multimode optical waveguide fabricated by UV cured epoxy resin for optical interconnection," in *Proc. 5th Asia-Pacific Conf./4th Optoelectron. Commun. Conf. Commun.*, 1999, vol. 2, pp. 1648–1651.
[40] M. Aktary, M. O. Jensen, K. L. Westra, M. J. Brett, and M. R. Freeman, "High-resolution pattern generation using the epoxy novolak SU-8 2000 resist by electron beam lithography," *J. Vacuum Sci. Technol. B, Microelectron. Nanometer Structures*, vol. 21, no. 4, pp. L5–L7, 2003.
[41] J. Hammacher, A. Fuelle, J. Flaemig, J. Saupe, B. Loechel, and J. Grimm, "Stress engineering and mechanical properties of SU-8-layers for mechanical applications," *Microsyst. Technol.*, vol. 14, no. 9, pp. 1515–1523, Oct. 01, 2008.
[42] A. Ane *et al.*, "SU-8-based microneedles for in vitro neural applications," *J. Micromech. Microeng.*, vol. 20, no. 6, p. 064014, 2010.
[43] Y. Wang *et al.*, "Surface graft polymerization of SU8 for bio-MEMS applications," *J. Micromech. Microeng.*, vol. 17, pp. 1371–1380, 2007.
[44] J. H. Lin *et al.*, "Giant enhancement of upconversion fluorescence of NaYF4:Yb3+,Tm3+ Nanocrystals with resonant waveguide grating substrate," *ACS Photon.*, vol. 2, no. 4, pp. 530–536, Apr. 15, 2015.
[45] S. Blair and Y. Chen, "Resonant-enhanced evanescent-wave fluorescence biosensing with cylindrical optical cavities," *Appl. Opt.*, vol. 40, no. 4, pp. 570–582, Feb. 1, 2001.
[46] Y. Jiang *et al.*, "Surface plasmon enhanced fluorescence of dye molecules on metal grating films," *J. Phys. Chem. C*, vol. 115, no. 25, pp. 12636–12642, Jun. 30, 2011.
[47] A.-H. Jalal, G. Marc Andre, and P. Muthukumaran, "Silicon-free, low-loss and high contrast polymer multimode waveguides," *J. Micromech. Microeng.*, vol. 27, no. 10, p. 105006, 2017.
[48] H. Kogelnik and V. Ramaswamy, "Scaling rules for thin-film optical waveguides," *Appl. Opt.*, vol. 13, no. 8, pp. 1857–1862, Aug. 1, 1974.
[49] W. Lukosz and R. E. Kunz, "Light emission by magnetic and electric dipoles close to a plane dielectric interface. II. Radiation patterns of perpendicular oriented dipoles," *J. Opt. Soc. Amer.*, vol. 67, no. 12, pp. 1615–1619, Dec. 1, 1977.
[50] C. K. Carniglia, L. Mandel, and K. H. Drexhage, "Absorption and emission of evanescent photons," *J. Opt. Soc. Amer.*, vol. 62, no. 4, pp. 479–486, Apr. 1, 1972.
[51] L. Novotny, "Allowed and forbidden light in near-field optics. I. A single dipolar light source," *J. Opt. Soc. Amer. A*, vol. 14, no. 1, pp. 91–104, Jan. 1, 1997.
[52] A. K. Wright and M. R. Thompson, "Hydrodynamic structure of bovine serum albumin determined by transient electric birefringence," *Biophys. J.*, vol. 15, no. 2, pp. 137–141, 1975.
[53] D. Marcuse, "Launching light into fiber cores from sources located in the cladding," *J. Lightw. Technol.*, vol. 6, no. 8, pp. 1273–1279, Aug. 1988.
[54] R. Srivastava, C. Bao, and C. Gómez-Reino, "Planar-surface-waveguide evanescent-wave chemical sensors," *Sensors Actuators A, Phys.*, vol. 51, no. 2, pp. 165–171, Nov. 1, 1995.
[55] H. Kogelnik and V. Ramaswamy, "Scaling rules for thin-film optical waveguides," *Appl. Opt.*, vol. 13, no. 8, pp. 1857–1862, Aug. 1, 1974.
[56] R. Bernini, N. Cennamo, A. Minardo, and L. Zeni, "Planar waveguides for fluorescence-based biosensing: Optimization and analysis," *IEEE Sensors J.*, vol. 6, no. 5, pp. 1218–1226, Oct. 2006.
[57] J.-H. Pai *et al.*, "A photoresist with low fluorescence for bioanalytical applications," *Anal. Chem.*, vol. 79, no. 22, pp. 8774–8780, Oct. 20, 2007.
[58] R. Walczak, P. Śniadek, and J. A. Dziuban, "SU-8 photoresist as material of optical passive components integrated with analytical microsystems for real-time polymerase chain reaction," *Optica Applicata*, vol. 41, no. 4, pp. 873–884, 2011.
[59] J. W. A. Findlay and R. F. Dillard, "Appropriate calibration curve fitting in ligand binding assays," *AAPS J.*, vol. 9, no. 2, pp. E260–E267, Jun. 2007.
[60] L. Liu, X. Zhou, J. S. Wilkinson, P. Hua, B. Song, and H. Shi, "Integrated optical waveguide-based fluorescent immunosensor for fast and sensitive detection of microcystin-LR in lakes: Optimization and analysis," *Sci. Rep.*, vol. 7, no. 1, p. 3655, Jun. 16, 2017.
[61] G. L. Long and J. D. Winefordner, "Limit of detection A closer look at the IUPAC definition," *Anal. Chem.*, vol. 55, no. 07, pp. 712A–724A, Jun. 1, 1983.